

POLARIZATION CONVERSION DEVICE BASED ON A WAVEGUIDE WITH PINS

V.Y.Dmytrenko¹, A.V. Bulashenko¹, S.I. Piltyay¹, O.V. Bulashenko²

¹Igor Sikorsky Kyiv Polytechnic Institute, Kyiv, Ukraine

²Ivan Kozhedub Shostka Professional College of Sumy State University
dmitrenkovitalina6@gmail.com, a.bulashenko@kpi.ua, crosspolar@ukr.net,
ol_bulashenko@ukr.net

Today, one of the key elements of antenna systems engaged in polarization signal processing are polarization devices. These devices are used to convert the types of polarization. The following designs of polarizers in the form of waveguide structures with posts [1], irises [2, 3], ridged structures [4], polarizers with thin metal septum [5] are known. The designs of polarizing devices in the form of slots [6] are complex in design. Phase shifters [7] and filters [8] also had such constructions. In addition, polarizers are built directly into antennas [9].

The 3-D model of the polarizer device is present in Fig. 1.

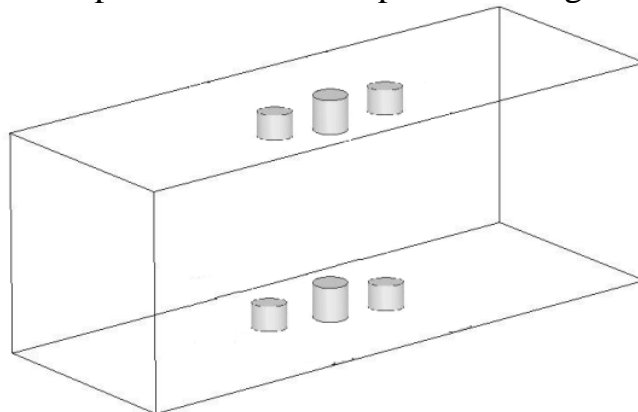


Figure. 1. 3-D model of the polarization conversion device

The design of the waveguide polarizer is shown in Fig. 2. The structure contains two posts of height h_1 and diameter d , one post of height h_2 and diameter d , the distance between the posts is l . Moreover, the height of the central post h_2 is greater than the height of the other posts h_1 .

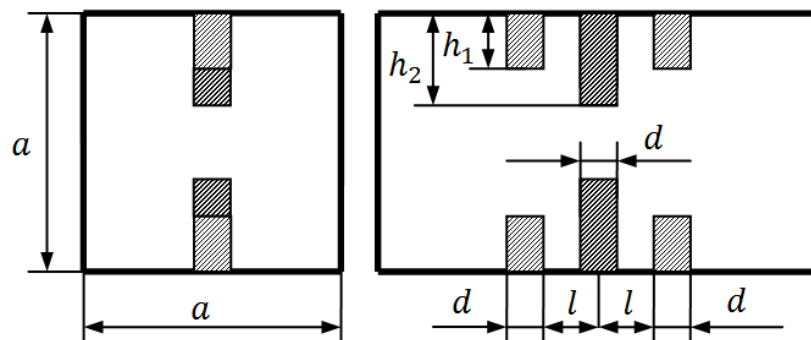


Figure. 2. Polarizer design based on a waveguide with three posts

The presence of a cylindrical post allows you to adjust the characteristics of the device by changing the length of the post.

The characteristics of the polarizer are as follows: phase, matching and polarization. Phase and matching are the differential phase shift and the voltage stand wave ratio (VSWR). The polarizing characteristics of a polarizer are the axial ratio and the crosspolar discrimination (XPD).

We form general wave matrices [10-12] on the basis of the theory of microwave, having broken the circuit of the polarizer into smaller circuits

$$[S_{\Sigma}] = \begin{bmatrix} S_{\Sigma 11} & S_{\Sigma 12} \\ S_{\Sigma 21} & S_{\Sigma 22} \end{bmatrix} = \frac{1}{T_{\Sigma 11}} \begin{bmatrix} T_{\Sigma 21} & |T| \\ 1 & -T_{\Sigma 12} \end{bmatrix},$$

$$[T_{\Sigma}] = [T_1] \cdot [T_2] \cdot [T_3] \cdot [T_4] \cdot [T_5] = \begin{bmatrix} T_{\Sigma 11} & T_{\Sigma 12} \\ T_{\Sigma 21} & T_{\Sigma 22} \end{bmatrix},$$

$$[T_2] = [T_4] = \begin{bmatrix} e^{j\theta} & 0 \\ 0 & e^{-j\theta} \end{bmatrix},$$

$$[T_1] = [T_5] = \frac{1}{2} \begin{bmatrix} 2 + Y_{p1} & -Y_{p1} \\ -Y_{p1} & 2 - Y_{p1} \end{bmatrix},$$

$$[T_3] = \frac{1}{2} \begin{bmatrix} 2 + Y_{p2} & -Y_{p2} \\ -Y_{p2} & 2 - Y_{p2} \end{bmatrix},$$

where Y_p is the conductivity of the post, θ is electric line length.

Differential phase shift is determined by the expression

$$\Delta\varphi = \varphi_{\Sigma 21,L} - \beta l.$$

VSWR is determined by the formula

$$VSWR = \frac{1 + |S_{11}|}{1 - |S_{11}|}.$$

The axial ratio is determined

$$r = 10 \lg \left(\frac{A^2 + B^2 + \sqrt{A^4 + B^4 + 2A^2B^2 \cos(\Delta\varphi)}}{A^2 + B^2 - \sqrt{A^4 + B^4 + 2A^2B^2 \cos(\Delta\varphi)}} \right),$$

where $A = 1$, $B = |S_{21}|$.

XPD is calculated by the formula

$$XPD = 20 \lg \left[\frac{10^{0.05r} + 1}{10^{0.05r} - 1} \right].$$

Fig. 3 shows the matching characteristics of the mathematical model, and Fig. 4 shows the polarization characteristics of this model.

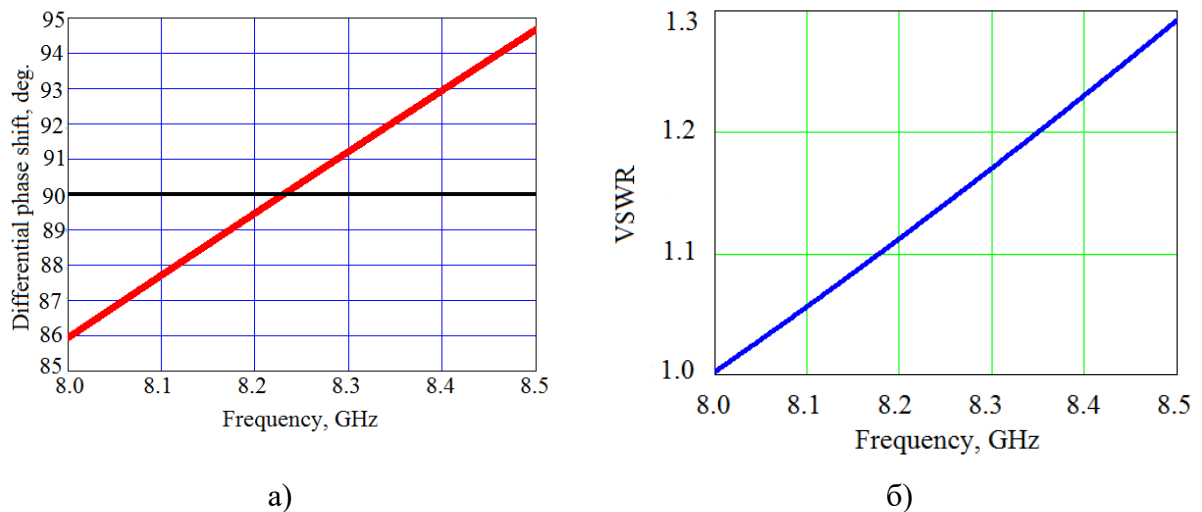


Figure 3. Matching characteristics of the mathematical model

Fig. 3a demonstrates that the maximum deviation of the differential phase shift from 90° is 4.5° . Fig. 3 b shows that the maximum value of VSWR is 1.28.

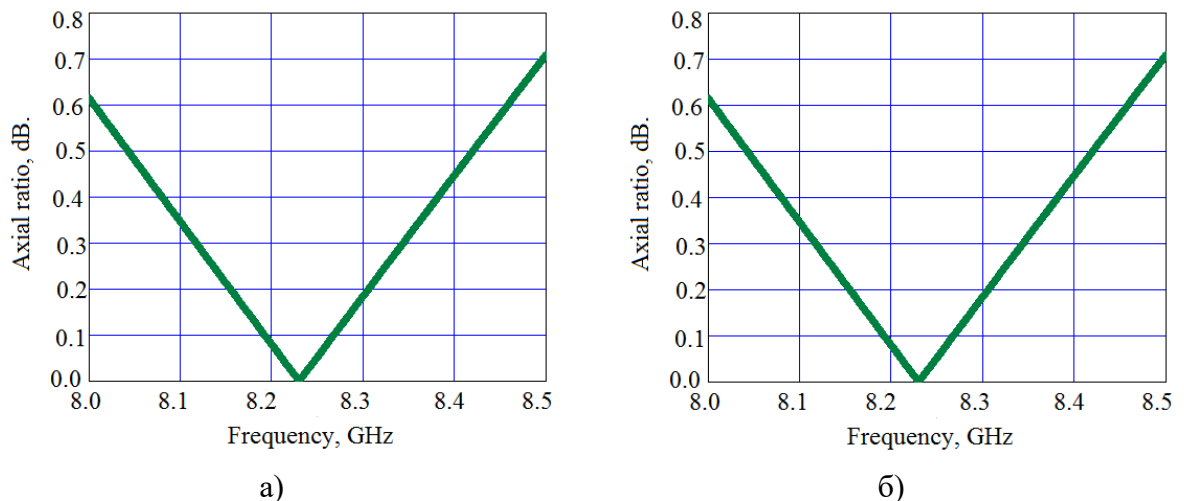


Figure 4. Polarization characteristics of the mathematical model

Fig. 4 a contains the dependence of the axial ratio on the frequency, and Fig. 4 b contains the dependence of the XPD on the frequency. From fig. 4 we see that at a frequency of 8.5 GHz the axial ratio acquires its maximum value of 0.71 dB. Also at this frequency, the XPD acquires a maximum value of 29 dB.

Fig. 5 shows the matching characteristics of the polarizer. Fig. 5 a contains the dependence of the differential phase shift on the frequency, and Fig. 5 b contains the dependence of VSWR on the frequency in the operating frequency range from 8.0 GHz to 8.5 GHz of the studied prototype.

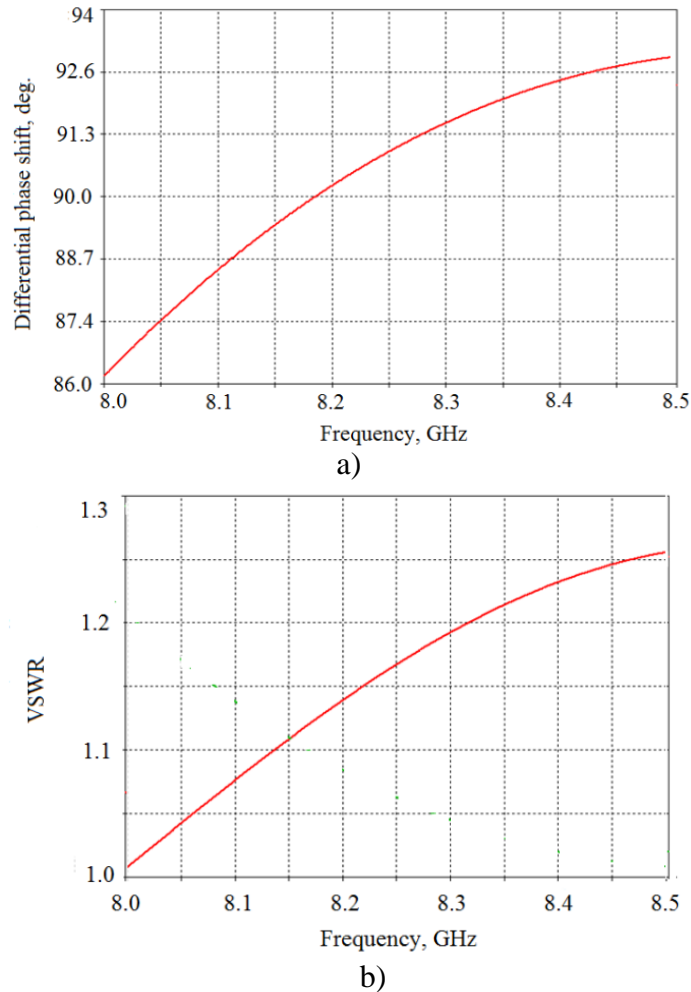


Figure 5. Matching characteristics of the prototype

Fig. 5a demonstrates that the maximum deviation of the differential phase shift from 90° is 4.2° . Fig. 5 b shows that the maximum value of VSWR is 1.26.

Fig. 6 shows the polarization characteristics of the device in the operating frequency range from 8.0 GHz to 8.5 GHz. Fig. 6 a contains the dependence of the axial ratio on the frequency, and Fig. 6 b contains the dependence of the XPD on the frequency. The figure shows that at a frequency of 8.0 GHz, the axial ratio acquires its maximum value of 0.55 dB. Also at this frequency, the XPD acquires a maximum value of 31 dB.

4. Tribak A. Ultra broadband low axial ratio corrugated quad-ridger polarizer / A.Tribak, A. Mediavilla, et al. // European Microwave Conferences, Rome, Italy. – October 2009. – pp. 284–287. DOI: 10.23919/EUMC.2009.5295927.
5. Deutschmann B. Broadband septum polarizer with triangular common port / B. Deutschmann, A.F. Jacob // IEEE Transactions on Microwave Theory and Techniques. – 2020. – Vol. 68, No. 2. – pp. 693-700. DOI: 10.1109/TMTT.2019.2951138.
6. Kulik D.Yu. Compact-size polarization rotators on the basis of irises with rectangular slots / D.Yu. Kulik,, A.O. Perov, N.G. Kolmakova // Telecommun. and Radio Engineering. – 2016. – Vol. 75, no. 10. – pp. 857-865, 2016. DOI: 10.1615/TelecomRadEng.v75.i10.10.
7. Qiu L.-L. Dual-band filtering differential phase shifter using cascaded wideband phase shifter and bandstop network with two same phase shifts / L.-L. Qiu and L. Zhu // IEEE Microwave and Wireless Components Letters. – 2021. – Vol. 31, no. 3. – pp. 261–264. DOI: 10.1109/LMWC.2020.3046247.
8. Omelianenko M.Y. Waveguide planar E-plane filter with ultra-wide stopband / M.Y. Omelianenko et al.// Radioelectron. Commun. Syst. – 2020. – Vol. 63, no. 12. pp. 650-655, 2020. DOI: 10.3103/S0735272720120031.
9. Wang K.X. A wideband millimeter-wave circularly polarized antenna with 3-D printed polarizer / K.X. Wang, H. Wong // IEEE Transactions on Antennas and Propagation. –2017. – Vol. 3. – pp. 1038–1046. DOI: 10.1109/TAP.2016.2647693.
10. Piltyay S.I. High performance waveguide polarizer for satellite information systems / S.I. Piltyay, A.V. Bulashenko, Ye.I. Kalinichenko, O.V. Bulashenko // Bulletin of Cherkasy State Technological University. – 2020. – Vol. 4. – pp. 14–26. [In Ukrainian], doi: 10.24025/2306-4412.4.2020.217129.
11. Bulashenko A.V. Tunable square waveguide polarizer with irises and posts / A.V. Bulashenko, et al. // Technical Engineering. – 2020. – Vol. 86, no 2. – pp. 108–116, doi: 10.26642/ten-2020-2(86)-108-116.
12. Bulashenko A.V. Simulation of compact polarizers for satellite telecommunication systems with the account of thickness of irises / A.V. Bulashenko, S.I. Piltyay, I.V. Demchenko // KPI Science news. – 2021. – Vol. 1. – pp. 7–15. DOI: 10.20535/kpispn.2021.1.231202.